J Mater Sci: Mater Med (2011) 22:2301–2309
DOI 10.1007/s10856-011-4405-5

Epitaxial growth of the zinc oxide nanorods, their characterization and in vitro biocompatibility studies

Ramya Gopikrishnan · Kai Zhang · Prabakaran Ravichandran · Santhoshkumar Biradar · Vani Ramesh · Virupaxi Goornavar · Robert B. Jeffers · Aswini Pradhan · Joseph C. Hall · Sudhakar Baluchamy · Govindarajan T. Ramesh

Received: 2 March 2011 / Accepted: 28 July 2011 / Published online: 7 August 2011

Abstract Here, we have synthesized Zinc Oxide (ZnO) nanorods at room temperature using zinc acetate and hexamethylenetetramine as precursors followed by characterization using X-ray diffraction (XRD), fourier transform infra red spectroscopy, scanning electron microscopy (SEM) and transmission electron microscopy. The growth of the synthesized ZnO was found to be very close to its hexagonal nature, which is confirmed by XRD. The nanorods were grown perpendicular to the long-axis and grew along the [001] direction, which is the nature of ZnO growth. The morphology of the synthesized ZnO nanorods was also confirmed by SEM. The size of the nanorod was estimated to be around 20–25 nm in diameter and approximately 50–60 nm in length. Our biocompatibility studies using synthesized ZnO showed no significant dose- or time-dependent increase in the formation of free radicals, accumulation of peroxidative products, antioxidant depletion or loss of cell viability on lung epithelial cells.

1 Introduction

Nanotechnology has extraordinary potential to change our lives by improving existing products and enabling new ones. Manufactured nanoparticles (NPs), whose structural elements have dimensions in the range of 1–100 nm, exhibit unique properties compared to the bulk material due to small size and large surface area relative to volume [1]. Due to their unique physical and chemical characteristics, these nanomaterials are being investigated for use in an increasing number of applications such as microelectronics, sensors, semiconductors and cosmetics as well as medical applications such as tissue engineering and drug delivery vehicles [2]. At the same time, these novel properties possessed by the materials at the nanoscale can lead to unpredictable outcomes in terms of their interactions with biological systems. This has been confirmed by a several studies in past few years concerning the undesirable side effects of nanoparticles exposure [3–5].

One class of nanostructures that has received recent attention is slender cylinders, variously referred to as nanoposts, nanorods and nanocolumns [6, 7]. Unintended exposure to nanomaterials may occur in occupational workers and end product users via inhalation, dermal absorption, or gastrointestinal tract absorption. Our previously published studies and other researchers have reported the adverse effects of nanomaterials with various compositions and properties on human health in vitro and in vivo settings [8–11].

Zinc oxide (ZnO) has unique properties; hence, it is used in a number of well-established biomedical applications. For example, ZnO nanorods grown on high electron mobility transistors devices have been shown to be highly sensitive for glucose detection [12], while ZnO has long been used as a dental filling materials [13], and sunscreens [14]. Because of the indiscriminate use of ZnO nanoparticles, it is important to look at their biocompatibility with biological system. Recently, studies on ZnO have shown that it induces much greater cytotoxicity than non-metal

R. Gopikrishnan · K. Zhang · P. Ravichandran · S. Biradar · V. Ramesh · V. Goornavar · R. B. Jeffers · A. Pradhan · J. C. Hall · G. T. Ramesh (✉)
Molecular Toxicology Laboratory, Center for Biotechnology and Biomedical Sciences, Department of Biology, Norfolk State University, Norfolk, VA 23504, USA
e-mail: gtramesh@nsu.edu

S. Baluchamy
Department of Biotechnology, Pondicherry University, Pondicherry 605014, India

nanoparticles on primary mouse embryo fibroblast cells [15], and induces apoptosis in neural stem cells [16]. A study on human aortic endothelial cells showed up-regulated mRNA levels of inflammatory markers on acute exposure of ZnO nanoparticles. Additionally, cell type-specific results have been reported [17]. Zinc oxide was reported to be nontoxic to cultured human dermal fibroblasts [18], and T-cells [19]. Whereas, it induced toxicity in neuroblastoma cells [20], BEAS-2B cell lines [21], and vascular endothelial cells [19], leading to the generation of reactive oxygen species (ROS), excitation of inflammation, and cell death.

In recent years, there has been an escalation in the development of techniques for synthesis of nanorods and subsequent surface functionalization. ZnO nanorods exhibit characteristic electronic, optical, and catalytic properties significantly different from other nano metals. Keeping in view, the unique properties and their extensive use of ZnO in many fields and also contradictory results on ZnO toxicity from both in vitro and in vivo, this study was performed. We present here the synthesis of ZnO nanorods at room temperature, characterization and biocompatible evaluation on lung epithelial cell line with no formation of free radicals, accumulation of peroxidative products, antioxidant depletion and the loss of cell viability.

2 Materials and methods

2.1 Chemicals

Zinc acetate anhydrous [$Zn(O_2CCH_3)_2$] and Hexamethylenetetramine ($C_6H_{12}N_4$) were purchased from Alfa Aesar (MA, USA), DMEM, Phosphate Buffered Saline (PBS), Fetal Bovine Serum (FBS), Hank's Balanced Salt Solution (HBSS), penicillin and streptomycin were obtained from Atlanta Biologicals, Inc. (Atlanta, GA). Glutathione (GSH), 3-(4,5-dimethylthiozol-2-yl)-2,5-diphenyl tetrazolium bromide (MTT), dimethylformamide (DMF), β-actin (Cat #A5441) and glutathione assay kit were obtained from Sigma Chemical Co. (St. Louis, MO). 2, 7-Dichlorofluorescein diacetate (DCF-DA) and Quick Apoptotic DNA ladder kit (Cat #: SKU-KHO1021) was purchased from Molecular Probes (Invitrogen Corporation, Carlsbad, CA). Lipid peroxidation assay kit was purchased from Cayman Chemicals (cat # 705002; Ann Arbor, MI). Superoxide Dismutase Kit was purchased from Trevigen, Inc. Gaithersburg, MD, USA (Cat # 7500-100-K). Coomassie plus protein assay reagent was purchased from Thermo fisher (cat # 1856210). Superoxide dismutase (SOD)-1 (sc 11407) antibody was obtained from Santa Cruz Biotechnology Inc. (Santa Cruz, CA, USA).

2.2 ZnO nanorod synthesis

The ZnO nanorods were synthesized as described earlier with a slight modification [22]. In a typical procedure, the aqueous zinc–hexamethylenetetramine (HMT) precursor was prepared by ultrasonicating $Zn(CH_3COO)_2{\cdot}2H_2O$ and HMT in 1:1 molar ratio, with the concentration of zinc ions being 0.1 mol/l, for about 20 min. After the mixture was mixed well, it was heated at 80°C in water bath for 90 min, during which white precipitates were deposited at the bottom. Next, hexamethylenetetramine was heated, where it decomposes into aldehyde and ammonia [23], which also produces OH^- ions. Following that Zn^{2+} was combined with OH^- to form Zn $(OH)_4^{2-}$ where it decomposed into ZnO after heating. The reaction formula is illustrated:

$$C_6H_{12}N_4 + 6H_2O \rightarrow 6CH_2O + 4NH_3$$
$$NH_3 + H_2O \rightarrow NH_4^+ + OH^-$$
$$Zn_2^+ + 4OH^- \rightarrow Zn\ (OH)_4^{2-} to ZnO$$

The reaction mixture was incubated for 35 min on ice cold water to terminate the reaction followed by several washes (until the pH becomes 7.0) using deionized water and alcohol to remove any by-product and excess hexamethylenetetramine. Finally, the purified ZnO nanorods were collected and dried at room temperature for 48 h. The white precipitated ZnO were used for further characterization. The commercially available ZnO (bulk ZnO from Sigma cat # 96479) was used as the standard for comparison with the prepared ZnO nanorods.

2.3 ZnO nanorods characterization

The microscopic characterization of ZnO nanorods was performed using transmission electron microscopy (TEM, JEM-2100, JEOL Instrument, Inc., Japan) and the scanning electron microscopy (SEM, JEOL JSM 5610LV). Nanorods of ZnO were suspended in ethanol and exposed to ultrasonic waves. For TEM method, one drop of the suspension was placed on 300 mesh copper grip, which was coated with holey carbon film followed by dehydration at 40°C. In case of SEM, the solution was dropped on a carbon tape followed by dehydration at 50°C. The structural characterizations were performed using a "Rigaku D-max" X-ray diffractometer (XRD) equipped with Cu Kα radiation ($\lambda = 1.541$ Å, 40 kV at 40 mA). The structural and molecular composition of nanorods was evaluated by Fourier transform infrared spectroscopy (PerkinElmer, FT-IR system spectrum GX) absorbance spectra. Samples were analyzed using an attenuated total reactance attachment from 500 to 4,000 cm^{-1}.

2.4 Cell culture and treatment

Rat Lung Epithelial (LE) cells (RL 65, CRL-10354) were purchased from American Type Culture Collection (Manassas, VA) and cultured in DMEM with 10% FBS, 100 IU/ml of penicillin, and 100 μg/ml of streptomycin and incubated at 37°C with 5% CO_2. For all the experiments, ZnO stocks (5 mg/ml) were prepared by dissolving in phosphate buffer saline (PBS) pH 7 and Single wall carbon nanotubes (SWCNT-1 μg/ml) was used as positive control. For control experiments, cells were treated with an equivalent volume of PBS.

2.5 Oxidative stress assay

The generation of ROS was measured using real time assay as described earlier [24]. The level of intracellular ROS was measured by the alteration of fluorescence resulting from oxidation of DCFH-DA. Briefly, LE cells (1×10^5 cells/well) were seeded in a 96-well plate and grown overnight at 37°C in a humidified chamber with 5% CO_2. The cells were then incubated with 10 μM of H_2DCF-DA with HBSS and incubated at 37°C for 3 h. Following incubation, cells were washed with PBS and treated with various concentrations of ZnO nanorods. At different time intervals, the intensity of fluorescence was measured at excitation and emission wavelengths of 485/527 nm, respectively, and the values were expressed as fluorescence units.

2.6 Cytotoxicity assays

The assay for cytotoxicity was performed using MTT, a tetrazole dye, as described earlier with slight modification [9]. Equal numbers of LE cells (2,000 cells/well) were seeded in a 96-well plate and grown overnight at 37°C in a humidified chamber with 5% CO_2. Briefly, following overnight growth, the cells were treated with different concentrations of ZnO nanorods and incubated for 48 h at 37°C. Thereafter, the cells were washed with PBS and MTT was added to a final concentration of 125 μg/ml and incubated for another 3 h at 37°C. The formazan formed inside the cells were extracted using acidic methanol and the absorbance was measured at 570 nm.

To reconfirm the cell viability results, a live-dead cell assay was performed essentially as described earlier [9]. Briefly, following treatment with 10 and 20 μg/ml of ZnO nanorods, approximately 10^5 cells were stained with Live/Dead reagent (5 μM ethidium homodimer, 5 μM calcein-AM, Molecular Probes, Eugene, OR) and incubated at 37°C for 30 min. The stained cells were analyzed under fluorescent microscope and photographed (Zeiss, Germany).

2.7 Lipid peroxidation assay

Lipid peroxidation level was measured using a kit from Cayman Chemicals as described earlier [10]. Equal numbers of LE cells (4×10^5 cells/well) were seeded in a 6-well plate and grown overnight at 37°C in a humidified chamber with 5% CO_2. Following incubation, cells were washed with PBS and treated with 10 and 20 μg/ml of ZnO nanorods and incubated for 24 h at 37°C. The cells were then centrifuged and proteins were estimated using coomassie plus protein assay reagent. Fifty micrograms of cell lysate was mixed with equal volume of pre-chilled methanol-chloroform mixture and centrifuged at $1{,}500 \times g$ for 10 min. The hydroperoxides present in the supernatant were collected and used for the estimation of LPO indicator malondialdehyde (MDA). Finally, freshly prepared chromogen was added and absorbance was measured at 500 nm.

2.8 Glutathione (GSH) assay

The concentration of intra cellular GSH was measured as described earlier [11]. In brief, equal numbers of LE cells (4×10^5 cells/well) were seeded in a 6-well plate and grown overnight at 37°C in a humidified chamber with 5% CO_2 The cells were then treated with 10 and 20 μg/ml of ZnO nanorods and incubated for 24 h at 37°C. Then, the cells were scraped and homogenized using PBS. Fifty microgram of protein was deproteinized using 5% 5-sulfosalicylic acid dihydrate solution and sodium carbonate (400 mM) followed by 1:8 dilutions with phosphate–EDTA buffer and incubated for 10 min at room temperature. The supernatant was then treated with 5, 5-di-thiobis (2-nitrobenzoic acid; DTNB) and incubated again at room temperature for 10 mins. The GSH activity was measured at 415 nm absorbance.

2.9 Superoxide dismutase assay

The concentration of intracellular total SOD was measured as described earlier [25]. Briefly, equal numbers of LE cells (4×10^5 cells/well) were seeded in 6-well plates and grown overnight at 37°C in a humidified chamber with 5% CO_2 The cells were then treated with 10 and 20 μg/ml of ZnO nanorods and incubated for 24 h at 37°C. Fifty microgram of protein extracts were used to assay total SOD activities using the manufacturer's protocol. Briefly, SOD reaction buffer was mixed with xanthine solution followed by NBT solution and then the sample proteins were added and the absorbance set to zero at 550 nm. Finally, XOD solution was added to each sample and readings were taken at 550 nm every 30 s for a period of 5 min. The total SOD

activity was measured according to the manufacturer's instruction.

2.10 Western blot analysis

Whole cell extracts were prepared from different time points of 15 μg/ml ZnO nanorods treated LE cells. Fifty microgram of proteins was separated using 10% SDS-PAGE and electro transferred to polyvinylidene difluoride membrane. Immunoblotting was performed by blocking overnight with 5% nonfat milk in PBS-0.1% NP40, probed with appropriate primary antibody followed by secondary antibody conjugated with horse radish peroxidase and developed using chemiluminescence reagent (GE Healthcare, Buckinghamshire, UK).

2.11 DNA fragmentation assay

DNA ladder analysis was performed as described earlier [26]. Genomic DNA was isolated from control and LE cells treated with 10 and 20 μg/ml of ZnO nanorods for 24 h using Quick Apoptotic DNA ladder kit. Briefly, treated and control LE cells were homogenized in TE buffer followed by mixing with buffered Tris-NaCl solution and incubated at 37°C for 10 min. Lysis buffer was added to the enzyme A mix and incubated for 30 min at 50°C water bath. To this, 1/10th volume of ammonium acetate and 2.5-fold cold ethanol were added and precipitated at −20°C for 15 min followed by centrifugation to get the DNA pellet. The pellet was washed with 70% cold ethanol and centrifuged again. Finally, the DNA was air-dried and resuspended in DNA suspension buffer and analyzed on 1.2% agarose gel.

2.12 Statistical analysis

For significant changes, data were analyzed by student's *t* test. A *P* value less than 0.05 was considered statistically significant.

3 Results

3.1 Characterization of ZnO nanorods

A typical powder XRD pattern of the synthesized ZnO nanorods is shown in Fig. 1. All of the peaks could be indexed to hexagonal Wurtzite-structured ZnO and close to the reported date (Joint Committee on Powder Diffraction Standards, Powder Diffraction File No. 36-1451; space group: $P6_3mc$ (186); $a = 0.3249$ nm, $c = 0.5206$ nm). Figure 2a, b shows a representative SEM morphology of the ZnO nanorods synthesized by the typical procedure. It can be seen that most of the ZnO nanorods have an average

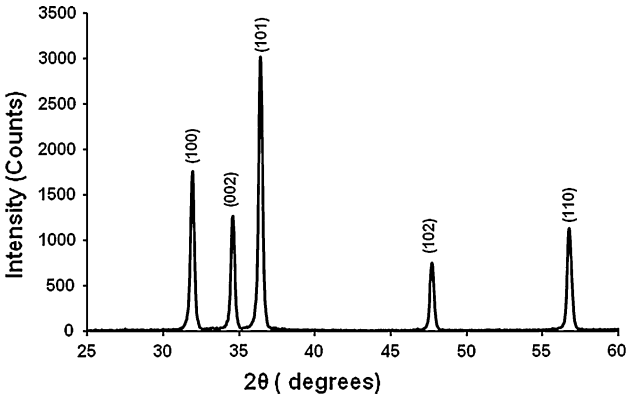

Fig. 1 X-ray diffraction patterns of ZnO nanorods

diameter range around 20–25 nm and a length of 50–60 nm, which shows the uniformity of the products. The morphology of ZnO from the individual crystalline nucleus was further confirmed by TEM image as shown in Fig. 2c, d. Figure 3 shows the Fourier transform infra red (FTIR) spectrum of synthesized ZnO nanorods with hexamethylenetetramine at room temperature. The characteristic absorbance was collected in the IR range from 4,000 to 400 cm^{-1}. A peak at ~418 cm^{-1} is the stretching vibration of the Zn–O bond in ZnO particles. The peaks at 2,857 cm^{-1} are assigned to the vibration of the C–H bond of the precursor.

3.2 Effect of ZnO on oxidative stress induction

Here, we examined the alteration of oxidative stress in LE cells. The cells were treated with different concentration (0.5, 1.0, 2.0, 2.5, 5.0, 10, and 20 μg/ml) of ZnO nanorods for 3 h and no significant induction of ROS was observed at concentration as high as 20 μg/ml as compared with the control (Fig. 4a). The time kinetics were also performed to check the formation of ROS and showed that ZnO nanorods induce no oxidative stress in a time- and dose-dependent manner in LE cells (Fig. 4b). No significant increase in ROS level was found even after 120 min. Next, we investigated the level of lipid peroxidation in ZnO nanorod exposed LE cells; another possible player for oxidative stress induction. As shown in Fig. 5, we observed no increase in lipid peroxidation level with 10 and 20 μg of ZnO nanorods, respectively as compared to control.

3.3 Inhibition of antioxidant levels in ZnO exposed cells

To evaluate the effect of ZnO nanorods on antioxidant, GSH level was checked on ZnO nanorod exposed LE cells (Fig. 6a). At 24 h, we observed no dose dependent depletion of GSH level as compared to control cells. In addition,

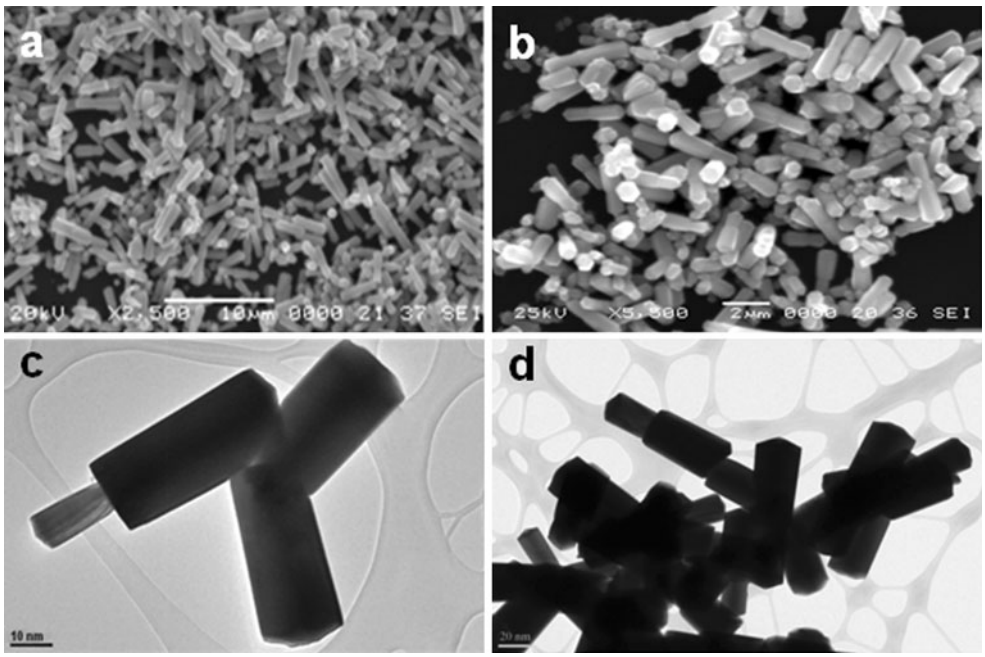

Fig. 2 Scanning Electron Micrograph of ZnO nanorods (**a**, **b**). Transmission Electron Micrograph of ZnO nanorods (**c**, **d**)

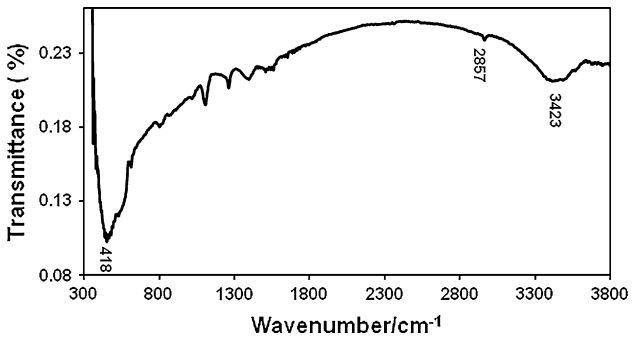

Fig. 3 FT-IR spectra of ZnO nanorods

we also observed no alteration of superoxide dismutase (SOD) levels in these cells as showed in Fig. 6b. Our immunoblot analysis from 15 μg ZnO exposed cells showed no change in the level of SOD-1 proteins even after 24 h (Fig. 6c).

3.4 ZnO effect on cell viability

Since, we observed no induction of oxidative stress and reduction of antioxidant levels in ZnO nanorod exposed LE cells, further we confirmed the biocompatibility of ZnO nanorods with LE cells using cell viability assay. MTT assay showed no concentration and time dependent cytotoxicity effect on ZnO exposed LE cells (Fig. 7a). To reconfirm the biocompatibility effect, live dead cell assay was performed. Fig. 7b shows there is no time dependent inhibition of cell viability in cells treated with 10 or 20 μg of ZnO nanorods as compared to control cells.

3.5 ZnO effect on DNA fragmentation

The DNA fragmentation is a key feature of programmed cell death and the process is characterized by the activation of endogenous endonucleases with subsequent cleavage of chromatin DNA into inter nucleosomal fragments of 180 base pairs and multiples thereof. Here we observed no fragmentation of DNA in cells treated with ZnO nanorods (Fig 8).

4 Discussion

Research on the biocompatibility of nano-sized structures requires appropriate characterizations of the material and their basic physiochemical information. Here, we report the synthesis of ZnO nanorods at room temperature using zinc acetate and hexamethylenetetramine as the precursors. The crystal structure of ZnO nanorod was measured with XRD. As seen in Fig. 1, the strongest detected (*h k l*) peaks are at $2\theta°$ values of 31.7°, 34.4°, 36.2°, 47.5° and 56.6° corresponding to the following lattice planes: (1 0 0) (0 0 2) (1 0 1) (1 0 2), and (1 1 0), respectively. No characteristic peaks of impurity phases such as Zn or $Zn(OH)_2$ were observed in our synthesis. Also, no diffraction peaks except ZnO were found. The XRD pattern indicate a (0 0 2)-preferred orientation, which suggests that the rods are quasi-aligned with the optical *c*-axis which is oriented perpendicularly to the substrate surface. The morphology and size of the ZnO nanorods were characterized by SEM and TEM. The SEM

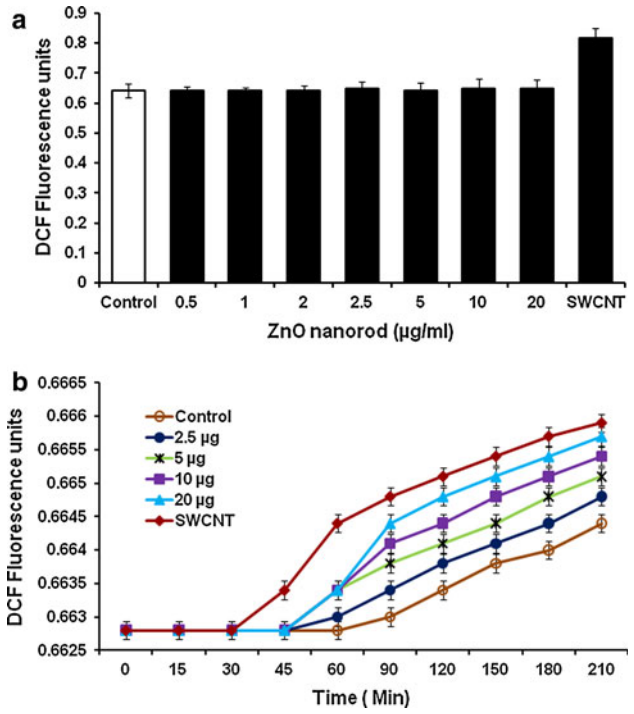

Fig. 4 Effect of ZnO nanorods on oxidative stress. Equal numbers of 1×10^5 LE cells/well were grown for 18 h. **a** The grown cells were incubated with 10 µM of DCF for 3 h, and then treated with different concentration of ZnO nanorods. Fluorescence was measured at excitation and emission wavelengths of 485 and 527 nm, respectively, at the end of 3 h. **b** Time kinetics of ROS formation by ZnO nanorods. Overnight grown LE cells were treated with 2.5, 5, and 10 µg/ml of ZnO nanorods. Fluorescence was measured at excitation and emission wavelengths of 485 and 527 nm, respectively, at different time points. The values are expressed as DCF fluorescence units, mean ± SD of eight wells and the figure is a representative of three experiments performed independently

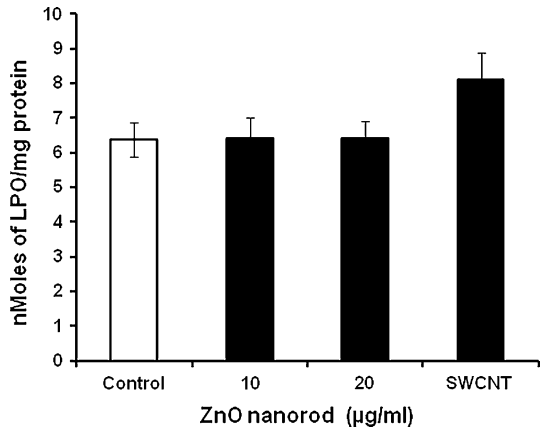

Fig. 5 Effect of ZnO nanorods on lipid peroxidation: 4×10^5 LE cells were grown for 24 h. Cells were then treated with 10 and 20 µg/ml of ZnO nanorods and allowed to grow for 24 h at 37°C. Lipid peroxidation levels were measured from chloroform–methanol extracts. The results represent the mean SD of three independent experiments

micrograph clearly shows that the nanorod was grown perpendicular to the long-axis of the matrix rod and grew along the [001] direction, which is the nature of ZnO growth, Fig. 2a, b). We have examined the TEM micrographs of samples prepared by the methods. As seen in Fig. 2c, d, most of the rods have a diameter of about 20–25 nm and a length of about 50–60 nm, which shows that products are uniform. The nanorod pointed by white arrow in Fig. 2a shows the general uniform hexagonal prismatic growth morphology of ZnO nanorods. The end surfaces should be {0 0 1} facets, which implies that [0 0 1] might be the growth direction. A similar morphology of ZnO was previously observed by [22].

When an infrared beam crosses a particle, the transmitted beam contains information not only on the interatomic bonds constituting the bulk, but also on the chemical groups at the particle surface. Though the latter are a minority by far, when the size of the particle is sufficiently decreased down to the nanometer scale, the concentration of the surface groups relative to that of the bulk interatomic bonds significantly increases and the contribution of these surface groups to the overall infrared absorption becomes no longer negligible [27]. The FTIR spectra of the synthesized ZnO nanorods with hexamethylenetetramine at room temperature were collected in the IR range from 4,000 to 400 cm^{-1} (Fig. 3). A broad absorption band at 3423 cm^{-1} in the IR spectra of ZnO particles can be seen, and these are attributed to the hydroxyl groups. Because the samples were immersed in the water during the growth of ZnO nanorods, the oxygen adsorbed to the surface would rather become O–H.

When investigating the biocompatibility of nanoparticles their size and shape are usually considered. Generally, the biological activity of particles increases as the particle size decreases. Smaller particles occupy less volume, resulting in a larger number of particles with a greater surface area per unit mass and increased potential for biological interaction [28]. Previous studies have demonstrated that particle size had no effect on toxicity of ZnO particles. Lin et al. found that the toxicity of 70 nm ZnO particles was similar to 420 nm ZnO particles [29]. Deng et al. showed 10, 30, 60 and 200 nm ZnO particles had similar toxicity to mouse NSC (C17.2) [16]. Yuan et al. also found 20, 30 and 40 nm ZnO particles had comparative toxicity in human embryonic lung fibroblasts (HELF) cells [30]. However, Nair et al. revealed that the toxicity of 40, 150 and 350 nm ZnO nanoparticles had a little difference in osteoblast cancer cells [31]. Thus; we inferred there may be a critical size, which could cause toxic effect to the living cells. Further studies are needed to prove this inference.

At present, there are few reports about the impact of ZnO particle shape on toxicity. One study has shown that

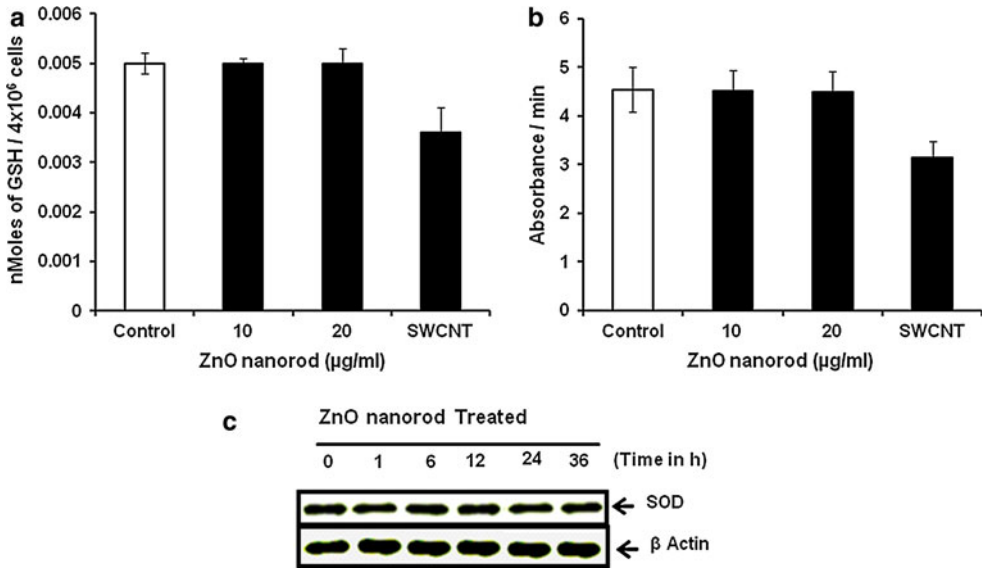

Fig. 6 Effect of ZnO nanorods on antioxidant levels (**a**, **b**). Equal numbers of 4×10^5 LE cells/well were grown for 24 h and treated with 10 and 20 µg/ml of ZnO nanorods and allowed to grow for additional 24 h. Total glutathione level was measured at 412 nm and the values were expressed in nanomoles and the superoxide dismutase activity was measured at 550 nm. Values are mean ± SD of three experiments performed independently. **c** Western blot showing SOD 1 protein in ZnO exposed LE cells. Cells were exposed to 15 µg of ZnO nanorods for various time points as indicated and proteins were resolved on SDS-PAGE and assayed for SOD1 using specific antibodies. The blots were stripped off and re probed with β-actin antibody for loading control

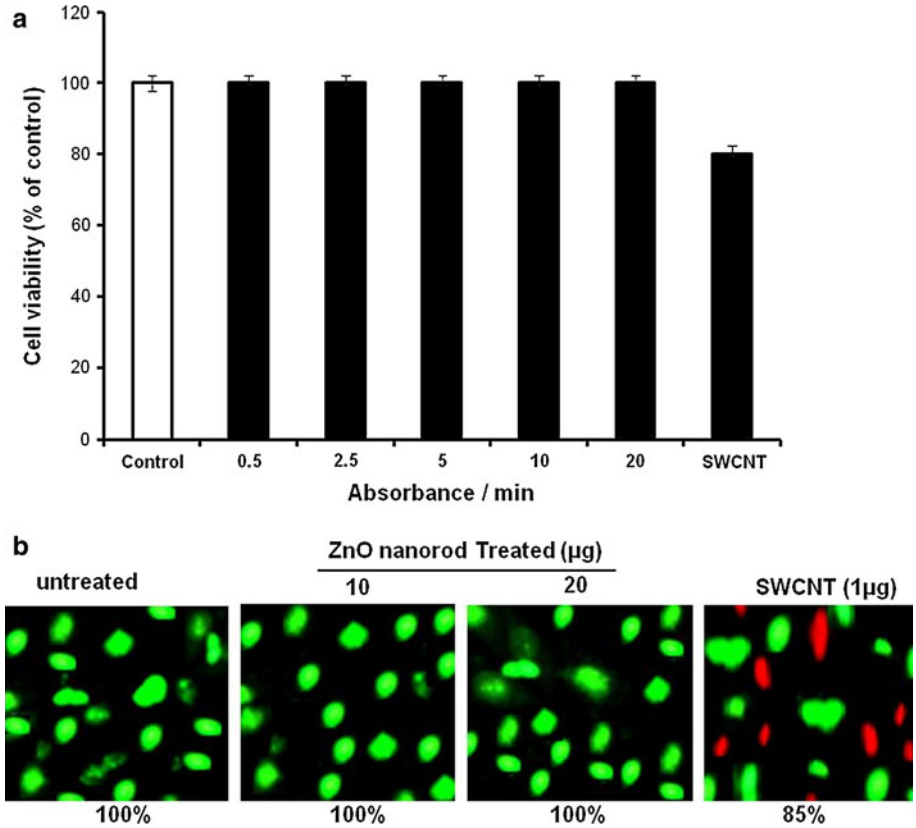

Fig. 7 Effect of ZnO nanorods on cell viability. LE cells (2,000/well in a 96-well plate) were grown for 12 h and treated with different concentration of ZnO nanorods and incubated for 48 h. **a** Cell viability was assayed by MTT dye uptake. The mean absorbance at 570 nm is represented as cell viability percentage of the control and is mean ± SD of eight wells. **b** LE cells were treated with 10 and 20 µg/ml of ZnO nanorods for 48 h. The percentage of live cells is indicated below

10–30 nm ZnO particles were spherical and 30 nm, 100 nm, and fine-ZnO particles were rod shaped. The 10–30 nm spherical ZnO particles were slightly more toxic than the three rod-like ZnO particles [32]. Thus, particle shape may affect its toxicity. Yang et al. inferred that the genotoxicity of different nanoparticles may primarily be

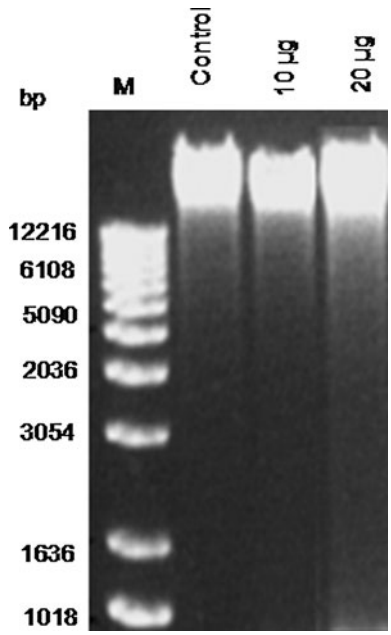

Fig. 8 Effect of ZnO nanorods on DNA fragmentation. Genomic DNA was extracted from LE cells treated with 10 and 20 µg of ZnO nanorods for 24 h and control cells using the quick apoptotic DNA ladder kit according to the manufacturer's instructions, analyzed on 1.2% agarose gel, and photographed

due to particle shape [15]. However in the study of Deng et al., the toxicity of 10 nm spherical ZnO particles was similar to 30 nm, 60 nm and 200 nm rod-like ZnO particles [16]. Therefore, the impact of particle size on the toxicity of ZnO nanoparticles needs further research.

It has been considered that dissolved zinc ions could play an important role in cytotoxicity [32]. ZnO is slightly soluble, and can release zinc ions into the solution. In order to study the effect of ZnO nanorods on LE cells, we measured intracellular ROS after exposure to ZnO nanorods. Increased level of oxidative damage causes a net stress on the normal body functions, leading to a gradual loss of vital physiological functions. ROS are the byproduct of normal cellular oxidative processes which has been suggested to regulate the process involved in initiation of apoptotic signaling [33]. Here, the time kinetics showed no significant increase in the intracellular ROS levels after exposure to ZnO nanorods which is in agreement with the cell viability and lipid peroxidation results. As shown in Fig. 5, we observed no increase in lipid peroxidation level with 10 µg/ml of ZnO nanorods as compared to the control. We observed no significant level of cell death even at the concentration of 10 µg ZnO nanorods after 48 h which was also confirmed by live dead cell assay (Fig. 7b). The possible reason for this condition could be that there is not enough free dissolved Zn^{2+} ions available to cause cytotoxicity. This result demonstrates that LE is biocompatible with synthesized ZnO nanorods which are supported by other findings. In contrast, previous studies have shown cytotoxicity of ZnO nanorods on mesothelioma MSTO-211H and HELF cells respectively [30, 34]. Also, 5 mM of ZnO nanoparticles are shown to be less toxic to human T cells [19]. Previous studies from our laboratory using single and multiwalled carbon nanotubes on cells such as lung epithelial, H1299, A549 and HaCaT cells showed the inhibition of cell viability suggesting their cytotoxic effects even at low concentration 5 µg/ml [9–11, 35].

ROS are known to react with DNA molecules causing damage to both purine and pyrimidine bases as well as the DNA backbone. Another important outcome of ROS production is lipid peroxidation which generates a variety of products reactive towards cellular macromolecules including DNA. Here, our results also show no significant induction of DNA fragmentation in ZnO exposed cells (Fig. 8). But previously, study conducted by Dufour et al. (2006) who have shown a concentration related increase in chromosome aberrations on ZnO NPs exposure (<100 nm) in CHO cells although at a very high concentration (≥105 µg/ml) [36].

Collectively, we have synthesized ZnO nanorods by mixing zinc acetate and hexamethylenetetramine and characterized using XRD; SEM, high resolution TEM, and FTIR spectroscopy. XRD measurements indicate that the synthesized nanorods are in the hexagonal wurtzite structure with high crystallinity and preferred growth direction of the *c*-axis. Our biocompatibility study supports the view that ZnO nanorods do not induce the formation of free radicals, the accumulation of peroxidative products, antioxidant depletion, the loss of cell viability and DNA fragmentation in LE cells. In summary, we report here the successful preparation of ZnO nanorods, characterization and biocompatibility studies on LE cells and conclude that ZnO nanorods could be a safe nanomaterial for biological applications.

Acknowledgments This work was supported by NASA funding NNX08BA47A: NCC-1-02038: NIH-1P20MD001822-1: NASA NSTI. This work was also supported by the NSF CREST.

References

1. Moriarty P. Nanostructured materials. Rep Prog Phys. 2001;64:297–381.
2. Nel A, Xia T, Madler L, Li N. Toxic potential of materials at the nano level. Science. 2006;311:622–7.
3. Brumfiel G. Nanotechnology: a little knowledge. Nature. 2003;424:246–8.
4. Goldston D. Small advances. Nature. 2007;450:1141.
5. Nielsen GD, Roursgaard M, Jensen KA, Poulsen SS, Larsen ST. In vivo biology and toxicology of fullerenes and their derivatives. Basic Clin Pharmacol Toxicol. 2008;103:197–208.
6. Kim W, Ng JK, Kunitake ME, Conklin BR, Yang P. Interfacing silicon nanowires with mammalian cells. J Am Chem Soc. 2007;129:7228–9.

7. Dalby MJ, Gadegaard N, Wilkinson CDW. The response of fibroblasts to hexagonal nanotopography fabricated by electron beam lithography. J Biomed Mater Res A. 2008;84:973–9.
8. Hsin Y, Chen C, Huang S, Shih T, Lai P, Chueh PJ. The apoptotic effect of nanosilver is mediated by a ROS- and JNK-dependent mechanism involving the mitochondrial pathway in NIH3T3 cells. Toxicol Lett. 2008;179:130–9.
9. Manna SK, Sarkar S, Barr J, Wise K, Barrera EV, Jejelowo O, Rice-Ficht AC, Ramesh GT. Single-walled carbon nanotube induces oxidative stress and activates nuclear transcription factor-kappaB in human keratinocytes. Nano Lett. 2005;5:1676–84.
10. Sharma CS, Sarkar S, Periyakaruppan A, Barr J, Wise K, Thomas R, Wilson BL, Ramesh GT. Single-walled carbon nanotubes induces oxidative stress in rat lung epithelial cells. J Nanosci Nanotechnol. 2007;7:2466–72.
11. Ravichandran P, Periyakaruppan A, Sadanandan B, Ramesh V, Hall JC, Jejelowo O, Ramesh GT. Induction of apoptosis in rat lung epithelial cells by multiwalled carbon nanotubes. J Biochem Mol Toxicol. 2009;23:333–4.
12. Kang BS, Wang HT, Ren F, Pearton SJ, Morey TE, Dennis DM. Enzymatic glucose detection using ZnO nanorods on the gate region of AlGaN/GaN high electron mobility transistors. Appl Phys Lett. 2007;91:252103–5.
13. Bodrumlu E. Biocompatibility of retrograde root filling materials: a review. Aust Endod J. 2008;34:30–5.
14. Nohynek GJ, Lademann J, Ribaud C, Roberts MS. Grey goo on the skin? Nanotechnology, cosmetic and sunscreen safety. Crit Rev Toxicol. 2007;37:251–77.
15. Yang H, Liu C, Yang D, Zhang HO, Xi Z. Comparative study of cytotoxicity, oxidative stress and genotoxicity induced by four typical nanomaterials: the role of particle size, shape and composition. J Appl Toxicol. 2009;29:69–78.
16. Deng X, Luan Q, Chen W, Wang Y, Wu M, Zhang H, Jiao Z. Nanosized zinc oxide particles induce neural stem cell apoptosis. Nanotechnology. 2009;20:115101.
17. Gojova A, Guo B, Kota RS, Rutledge JC, Kennedy IM, Barakat AI. Induction of inflammation in vascular endothelial cells by metal oxide nanoparticles: effects of particle composition. Environ Health Perspect. 2007;155:403–9.
18. Agren MS, Mirastschijski U. The release of zinc ions from and cytocompatibility of two zinc oxide dressings. J Wound Care. 2004;13:367–9.
19. Reddy KM, Feris K, Bell J, Wingett DG, Hanley C, Punnoose A. Selective toxicity of zinc oxide nanoparticles to prokaryotic and eukaryotic systems. Appl Phys Lett. 2007;90:213902.
20. Jeng HA, Swanson J. Toxicity of metal oxide nanoparticles in mammalian cells. J Environ Sci Health A. 2006;41:2699–711.
21. Xia T, Kovochich M, Liong M, Madler L, Gilbert B, Shi H, Yeh JI, Zink JI, Nel AE. Comparison of the mechanism of toxicity of zinc oxide and cerium oxide nanoparticles based on dissolution and oxidative stress properties. ACS Nano. 2008;10:2121–34.
22. Tang J, Yang X. An one-pot epitaxial growth method to synthesize cactus-like ZnO. Mater Lett. 2006;60:3487–91.
23. Strom JG, Jun HW. Kinetics of hydrolysis of methenamine. J Pharm Sci. 1980;69:1261–3.
24. Sarkar S, Sharma C, Yog R, Periakaruppan A, Jejelowo O, Thomas R, Barrera EV, Rice-Ficht AC, Wilson BL, Ramesh GT. Analysis of stress responsive genes induced by single-walled carbon nanotubes in BJ Foreskin cells. J Nanosci Nanotechnol. 2007;7:584–92.
25. Baluchamy S, Ravichandran P, Periyakaruppan A, Ramesh V, Hall JC, Zhang Ye, Gridley SD, Jejelowo O, Wu H, Ramesh GT. Induction of cell death through alteration of oxidants and anti-oxidants in lung epithelial cells exposed to high energy protons. J Biol chem. 2010;285:24769–74.
26. Ravichandran P, Baluchamy S, Sadanandan B, Gopikrishnan R, Biradar S, Ramesh V, Hall JC, Ramesh GT. Multiwalled carbon nanotubes activate NF-κB and AP-1 signaling pathways to induce apoptosis in rat lung epithelial cells. Apoptosis. 2010;15:1507–16.
27. Prasad V, Souza CD, Yadav D, Shaikh AJ, Vigneshwaran N. Spectroscopic characterization of zinc oxide nanorods synthesized by solid state reaction. Spectrochim Acta A Mol Biomol Spectrosc. 2006;65:173–8.
28. Oberdörster G, Stone V, Donaldson K. Toxicology of nanoparticles: a historical perspective. Nanotoxicology. 2007;1:2–25.
29. Lin W, Xu Y, Huang CC, Ma Y, Shannon KB, Chen DR, Huang YW. Toxicity of nano- and micro-sized ZnO particles in human lung epithelial cells. J Nanopart Res. 2009;11:25–39.
30. Yuan JH, Chen Y, Zha HX, Song LJ, Li CY, Li JQ, Xia XH. Determination, characterization and cytotoxicity on HELF cells of ZnO nanoparticles. Colloids Surf B Biointerfaces. 2010;76:145–50.
31. Nair S, Sasidharan A, Divya Rani VV, Menon D, Nair S, Manzoor K, Raina S. Role of size scale of ZnO nanoparticles and microparticles on toxicity toward bacteria and osteoblast cancer cells. J Mater Sci Mater Med. 2009;20:S235–41.
32. Songa W, Zhangb J, Guoa J, Zhanga J, Dingc F, Li L, Suna Z. Role of the dissolved zinc ion and reactive oxygen species in cytotoxicity of ZnO nanoparticles. Toxicol Lett. 2010;199:389–97.
33. Waris G, Ahsan H. Reactive oxygen species: role in the development of cancer and various chronic conditions. J Carcinogen. 2006;5:1–8.
34. Brunner TK, Wick P, Manser P, Spohn P, Grass PN, Limbach L, Bruinink A, Stark WJ. In vitro cytotoxicity of oxide nanoparticles: comparison to asbestos, silica, and the effect of particle solubility. Environ Sci Technol. 2006;40:4374–81.
35. Ravichandran P, Baluchamy S, Gopikrishnan R, Biradar S, Ramesh V, Goornavar V, Thomas R, Wilson BL, Jeffers R, Hall JC, Ramesh GT. Pulmonary biocompatibility assessment of inhaled single-wall and multi-wall carbon nanotubes in BALB/c mice. J Biol Chem. 2011. doi:10.1074/jbc.M111.251884.
36. Dufour EK, Kumaravel T, Nohynek GJ, Kirkland D, Toutain H. Clastogenicity, photo-clatogenicity or pseudo-photo-clastogenicity: genotoxic effect of zinc oxide in the dark, in pre-irradiated or simultaneously irradiated Chinese hamster ovary cells. Mutat Res. 2006;607:215–24.